



TITLE:

Experimental Studies on the Elastic-Plastic Behavior of Braced Frames under Repeated Horizontal Loading. Part 3 Experiments of One Story-One Bay Braced Frames

AUTHOR(S):

WAKABAYASHI, Minoru; NAKAMURA, Takeshi;
YOSHIDA, Nozomu

CITATION:

WAKABAYASHI, Minoru ...[et al.]. Experimental Studies on the Elastic-Plastic Behavior of Braced Frames under Repeated Horizontal Loading. Part 3 Experiments of One Story-One Bay Braced Frames. Bulletin of the Disaster Prevention Research Institute 1980, 29(4): 143-164

ISSUE DATE:

1980-03

URL:

<http://hdl.handle.net/2433/124888>

RIGHT:

Experimental Studies on the Elastic-Plastic Behavior of Braced Frames under Repeated Horizontal Loading

Part 3 Experiments of One Story-One Bay Braced Frames

By MINORU WAKABAYASHI, Takeshi NAKAMURA and NOZOMU YOSHIDA

(Manuscript received December 27, 1979)

Abstract

Experimental studies have been conducted to investigate the hysteretic behavior of one story-one bay braced steel frames whose braces are made of built-up H-shapes and whose columns and beams are made of rolled H-shapes. Hysteretic behavior and transition and change of load carrying capacity of each component member of a frame, i.e., braces, columns and beams under repeated horizontal load are examined individually as well as the hysteretic behavior of a braced frame as a whole. Interaction behavior between the braces built in a frame and the components of the surrounding frame is also discussed. As a fruit of the investigation, the following is remarked. The effective slenderness ratio for buckling of the braces built in a frame could be estimated by the slope-deflection method taking the rotational rigidity by the members of the surrounding frame into account. Since hysteretic behavior of the braces built in the surrounding frame, the dimensions of whose component members are comparable with those of the brace is not much different from that of the brace reported in Part 1¹⁾ which was approximately rigidly fixed in the heavy surrounding frame, the effect of the deformation of the members of the surrounding frame on the hysteretic behavior of the brace would not be large. The effective slenderness ratio for the estimation of the post-buckling and hysteretic behaviors could be approximated by the assumption that the braces would be rigidly fixed at the ends. As the columns are subjected to large repeated axial load due to the deformation of the brace and the load carrying capacity of the column largely decreases when the axial load is large, the behavior of the column is largely affected by that of the brace. The load carrying capacity and the ductility of the brace are reduced and exhausted when cracks are initiated as well as reported in Part 1¹⁾ and Part 2²⁾.

1. Introduction

An elastic-plastic behavior of one story-one bay braced steel frames and their components such as braces and columns under repeated horizontal loading is discussed on the basis of experimental investigation. The objectives of this series of experimental studies are to clarify the hysteretic behavior of the existing steel braces and bracing systems and to grasp the behavior of braces up to failure and up to breakage, aiming at the formulation of a hysteretic rule of the restoring force characteristics of the braces and the establishment of the earthquake-resistant design method of bracing systems. In Part 1 and Part 2 of the reports of this experimental series, the results of the test of various types of braces made of built-up H-shapes, angle shapes, steel tubes, flat bars and round bars which are put in the frame which does not resist any horizontal load were reported. In this paper, one story-one bay braced frames are treated. The cross sectional shape of the brace is an H-shape and the nominal dimensions and details in design of the braces are similar to those reported in Part 1.

The brace is welded to a surrounding frame made of rolled H-shapes without eccentricity. Hysteretic behavior of the braces and the columns of the surrounding frame is investigated in detail as well as that of the whole system. Finally, the treatment of the braces in an actual design is discussed comparing the behavior of the braces in a braced frame of the present test with that of the braces reported in Part 1.

2. Test Plan

2.1 Planning of Test

The experiment was planned and performed to examine the hysteretic behavior of externally simply supported one story-one bay braced frames subjected to repeated horizontal loading in a quasi-static manner. Beams and columns of the test specimens were made of H-shapes which were the most widely used steel members in the actual steel structures. Braces were also made of H-shapes. Nominal dimensions of the brace were identical with those of the brace specimens whose behavior was reported in Part 1¹⁾ of this series of experimental investigation, so as to make the direct comparison of the test results possible. The main parameters of the test are as follows.

a) Types of Bracing

Single and double bracing systems which are shown in the circles in **Fig. 1** are the objects to be investigated and called Z-type bracing system and X-type bracing system in this report, respectively. A pure rigid frame without braces is also tested.

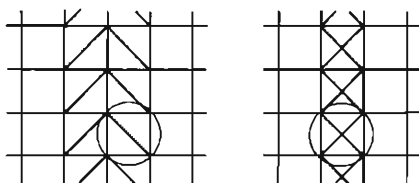


Fig. 1. Extraction of the Model of the Test Frame.

b) Plane of Buckling of Braces

The weak axis of a cross section of a brace is put in the plane of a frame or in the plane perpendicular to the plane of a frame. In the former specimen, the brace is designed to buckle out of the plane of a frame and in the latter specimen the brace is designed to buckle in the plane of a frame.

2.2 Test Specimen

Columns and beams of the test specimen were made of JIS-SS 41 grade hot rolled H-shapes with 100 mm depth, 100 mm flange width, 6 mm web thickness and 8 mm flange thickness (H-100×100×6×8). Braces were built-up H-shapes. Each plate element of the brace is made of hot rolled steel plate of JIS-SS 41 grade with 6 mm thickness. The plates were built up to an H-shape by fillet-welding with 2 mm leg length. The dimensions of a cross section of the brace are 50 mm in depth, 50 mm in width of flanges and 6 mm in thickness of web and flanges (Built-up H-50×50×6×6). Test frames were annealed to remove the residual stress due to

manufacturing. Mechanical properties of the used steel plate and H-shapes which were obtained from tensile tests and stub column tests of the coupon specimens are tabulated in **Table 1**. Totally five specimens were tested. The general configuration of the specimens are illustrated in **Fig. 2** and their measured dimensions are tabulated in **Table 2**. Peculiarity of each specimen is as follows.

Table 1. Results of Material Tests

Specimens			Tension Tests				Stub Column Tests
			σ_y (t/cm ²)	σ_u (t/cm ²)	ϵ_{st}	ϵ_u	σ_y (t/cm ²)
Brace			2.75	4.17	0.024	0.39	
Columns and Beams	BFOF	Flange	2.54	4.30	0.023	0.26	2.56
		Web	2.81	4.32	0.028	0.31	
	BFSI	Flange	2.74	4.55	0.032	0.32	2.85
		Web	2.91	4.35	0.023	0.28	
	BFSO	Flange	2.54	4.30	0.023	0.26	2.58
		Web	2.81	4.32	0.028	0.31	
	BFDI	Flange	2.54	4.30	0.023	0.26	2.55
		Web	2.81	4.32	0.028	0.31	
	BFDO	Flange	2.47	4.20	0.023	0.36	2.51
		Web	2.82	4.29	0.023	0.38	

Table 2. Measured Dimensions of the Test Specimens

Specimens		BFOF	BFSI	BFSO	BFDI	BFDO
Column ①	H (mm)	100.3	100.6	100.9	100.4	99.4
	B (mm)	99.6	100.4	100.0	99.9	100.0
	t_w (mm)	5.73	5.68	5.52	5.68	5.62
	t_f (mm)	7.50	7.61	7.51	7.53	7.54
Column ②	H (mm)	99.0	99.3	99.0	99.3	100.3
	B (mm)	99.8	100.4	99.7	99.9	99.9
	t_w (mm)	5.73	5.68	5.52	5.65	5.60
	t_f (mm)	7.46	7.65	7.52	7.55	7.54
Beam ①	H (mm)	100.3	100.6	100.6	99.2	100.2
	B (mm)	99.9	100.4	99.7	99.8	99.8
	t_w (mm)	5.78	5.62	5.63	5.63	5.78
	t_f (mm)	7.49	7.61	7.51	7.53	7.52
Beam ②	H (mm)	100.4	99.2	98.8	99.2	99.4
	B (mm)	99.7	100.4	99.9	99.9	99.7
	t_w (mm)	5.75	5.65	5.62	5.93	5.57
	t_f (mm)	7.50	7.61	7.50	7.53	7.53
Brace ①	H (mm)		49.4	49.6	50.0	49.6
	B (mm)		49.6	49.7	49.9	50.0
	t_w (mm)		5.93	5.89	5.93	6.09
	t_f (mm)		5.92	6.10	6.08	5.99
Brace ②	H (mm)				50.1	49.4
	B (mm)				49.7	49.8
	t_w (mm)				5.94	6.08
	t_f (mm)				6.02	5.98

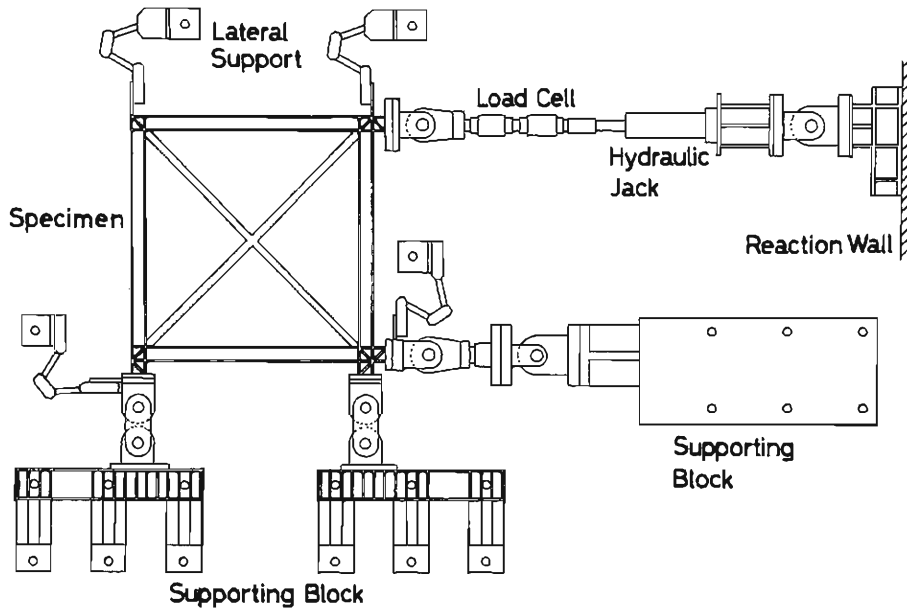


Fig. 3. Test Set-up.

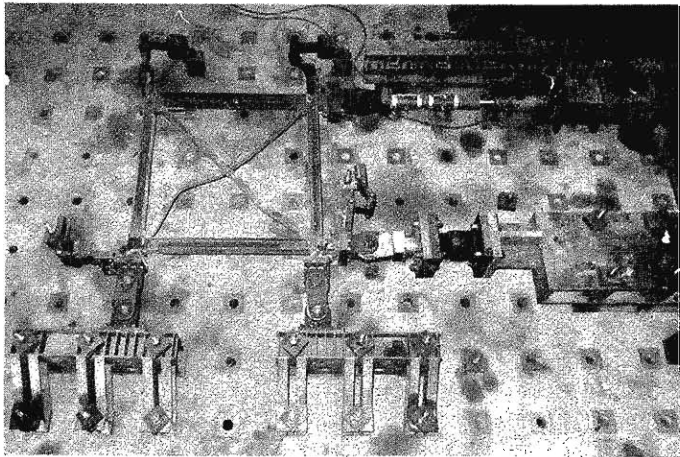


Photo. 1. General View of the Experiment.

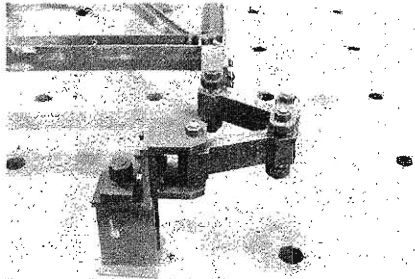


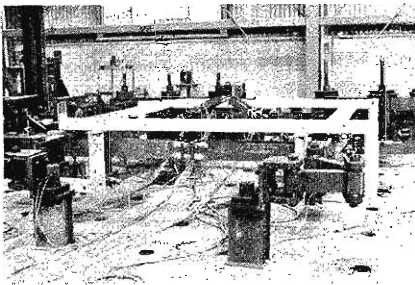
Photo. 2. Lateral Support at the Beam-to-Column Connection.

designed to buckle in the plane perpendicular to the plane of a frame.

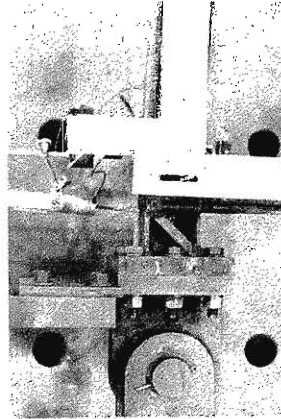
BFDI : A braced frame with X-type double bracing system. The braces are designed to buckle in the plane of a frame.

BFDO: A braced frame with X-type double bracing system. The braces are designed to buckle in the plane perpendicular to the plane of a frame.

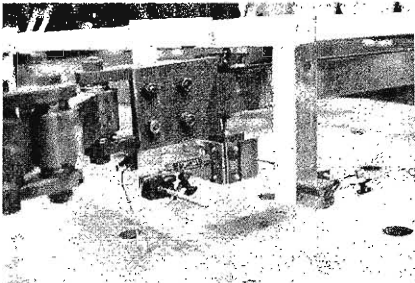
2.3 Test Set-up and Measurement



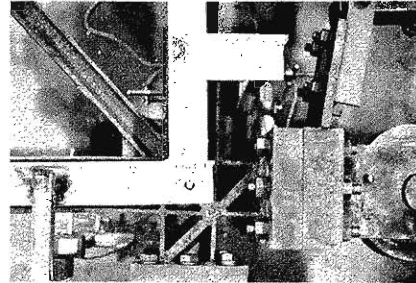
(a) The Frame for Measurement of Deflection.



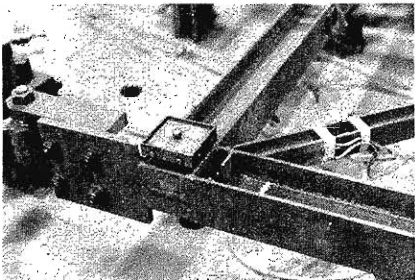
(d) Roller Supports.



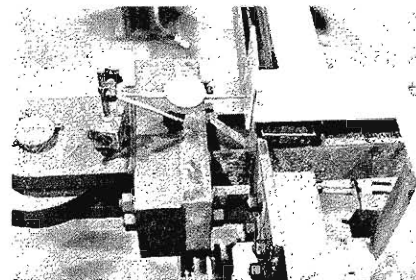
(b) Deflection Measurement at the Beam-to-Column Connection.



(e) Pinned Supports.



(c) Pinned Support for the Frame for Measurement.



(f) Measuring of Story Drift.

Photo. 3. Test Equipment.

Figure 3 shows the test set-up schematically and the general view of the experiment is shown in **Photo. 1**. The test specimens were supported by three roller-supports at the beam-to-column connections. Since one of them sustains the horizontal force and other two sustain the vertical forces, the test frame is simply supported on the reaction floor, as shown in **Figs. 3** and **5**. The movement out of the plane of the test frame was prevented by four lateral supports which were set near the beam-to-column connections, as shown in **Fig. 3** and **Photo. 2**. Horizontal load was given by a 50 ton push-pull-type static hydraulic jack and measured by two load cells which were inserted between the test frame and the hydraulic jack. A frame to measure displacements and deformation were set on the test frame as shown in **Photo. 3** to obtain the relative horizontal and vertical displacements and the rotation at the two free nodes of the specimen, the relative horizontal displacement and the rotation at the roller-supported node and the relative rotation at the pin-supported node. Relative horizontal movement (Δ) between this frame and the point where the load is applied are measured by a dial gage (**Photo. 3**). Four pieces of electric resistance strain gage for a section are mounted at two sections in the beams and columns of the specimen which are 5 cm apart from the mid-length to measure a longitudinal stress and a bending moment distribution along the longitudinal axis.

2.4 Loading program

The loading program is identical with that of the previously reported test^(1),2). The loading is controlled on the basis of the amplitude of story drift angle (R) which is the ratio of story drift (Δ) to the clear height of a column (1.4 meters in nominal dimension). The programmed amplitude of story drift angle (R_d) versus the number of loading cycle relationship is shown in **Fig. 4**.

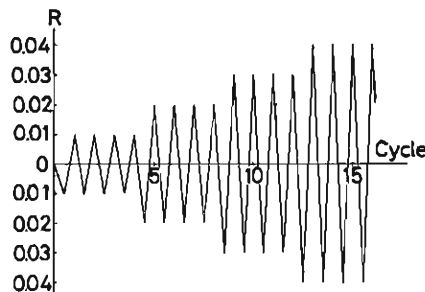


Fig. 4. Loading Program.

3. Behavior of Each Specimen in the Experiments

The behaviors of each specimen observed in the test are described in this section. Each member and node of the frame are hereinafter referred to as shown in **Fig. 5** for convenience of explanation. Experimental horizontal force (H) versus story drift (Δ) relationships are shown in **Figs. 6~10**.

1) BFOF

This is a pure rigid frame specimen. Experimental restoring force (H) versus story drift (Δ) relationship is shown in **Fig. 6**. H - Δ relation is linear in the loading

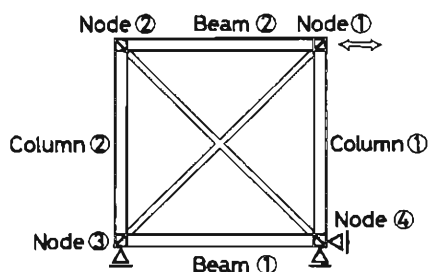
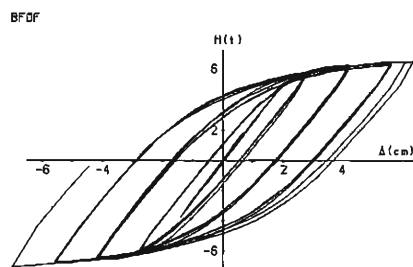
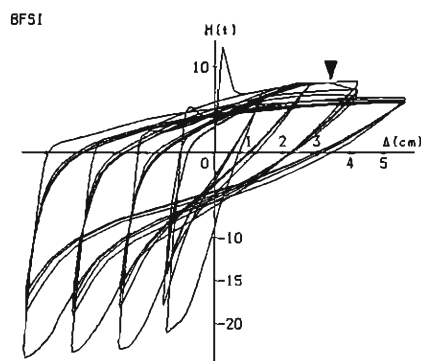
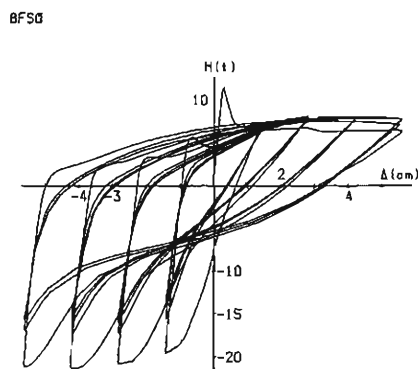
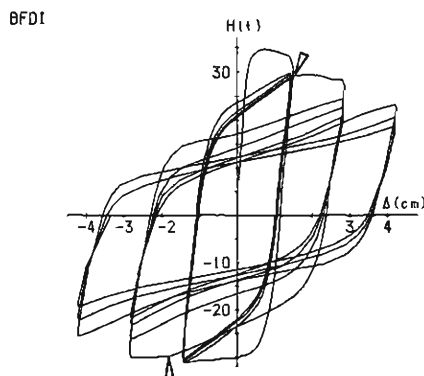
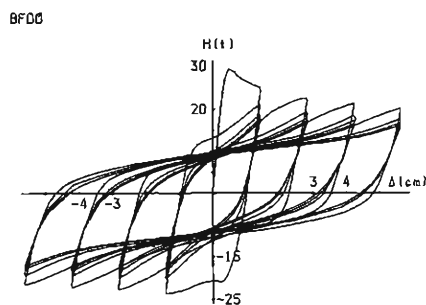


Fig. 5. Names of the Members and Nodes.

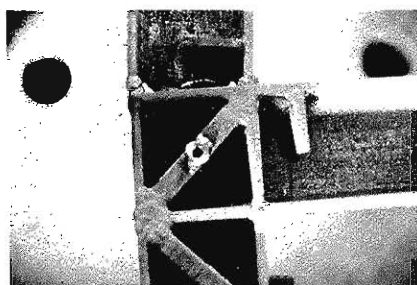
Fig. 6. H - Δ Relationship of BFOF.Fig. 7. H - Δ Relationship of BFSI.Fig. 8. H - Δ Relationship of BFSO.Fig. 9. H - Δ Relationship of BFDI.Fig. 10. H - Δ Relationship of BFDO.

range of $R_A=0.01$ and the specimen is in an elastic state. In the range $R_A=0.01$, the specimen begins to be plastified gradually and the H - Δ relationship shows hysteresis loops with a spindle shape. The hysteresis loop is stable and the deterioration of the load carrying capacity due to cyclic loading is not observed through the whole process of loading.

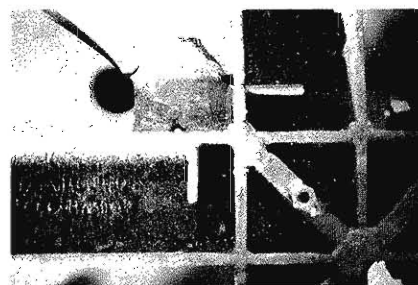
2) BFSI

This is the single bracing type specimen whose brace was designed to buckle in the plane of a frame and H - Δ relationship is shown in Fig. 7. The maximum load

carrying capacity is reached at about $\Delta = 0.255$ cm ($R = 0.17 \times 10^{-2}$ rad.) in the virgin loading stage in which the brace is subjected to compressive force and the load carrying capacity decreases rapidly according to the buckling of the brace. The decrease of the load carrying capacity occurs at about $H = 6.825$ ton and $\Delta = 0.85$ cm ($R = 0.57 \times 10^{-2}$ rad.), then the load carrying capacity again increases gradually. This re-increase of the load carrying capacity after deterioration is recognized when considering that the decreasing rate of the load carrying capacity of a brace which has been extraordinarily large in the range just after the buckling becomes less gradually as the story-drift becomes larger, and finally it becomes smaller than the increasing rate of the load carrying capacity of the column which is in the elastic state and the load capacity carried by the whole system, which is represented by the sum total of load capacities by a brace and columns, increases gradually. The behavior such that the load carrying capacity once decreases and again increases with the increase of the story drift is observed whenever the loading amplitude R_d is enlarged, although the decrease of the load carrying capacity is not so rapid as in the first cycle. The hysteresis loop has the shape of a boomerang after the second cycle of loading in each loading amplitude. Cracks take place in the flange of the column ② near node ③ where the column is connected to the beam by butt-welding, in the 10th cycle of loading ($R_d = 0.03$, $H = 7.45$ t, $\Delta = 4.06$ cm, $R = 2.71 \times 10^{-2}$ rad.). Crack initiation is shown by a mark ▼ in Fig. 7. The cracks grows and reaches to the web (Photo. 4a) in the subsequent loading and the deterioration of the load carrying capacity becomes larger. Cracks also take place at the end of the brace (Photo. 4b) in the 13th cycle ($H = -21.2$ t, $\Delta = -4.83$ cm, $R = 3.22 \times 10^{-2}$ rad.), as shown in Photo. 4(b).



(a) Crack at the End of Column.



(b) Crack near the End of Brace.

Photo. 4. Cracks in BFSI.

3) BFSO

This is the single bracing type specimen whose brace was designed to buckle in the plane perpendicular to the plane of a frame. Experimental $H-\Delta$ relationship is shown in Fig. 8. The behavior of this specimen is quite similar to that of the specimen named BFSI except that the planes of buckling of the brace are different. The maximum load carrying capacity is $H = 11.45$ t at $\Delta = 0.315$ cm ($R = 0.21 \times 10^{-2}$ rad.) and the re-increase of the load carrying capacity begins at about $\Delta = 1.1$ cm ($R = 0.73 \times 10^{-2}$ rad.) ($H = 6.825$ t) in the first cycle of loading. The hysteresis loops after the second cycle have a shape like a boomerang. Cracks took place at the same portion as BFSI in the 15th cycle of loading ($H = 7.475$ t, $\Delta = 2.6$ cm, $R = 1.73 \times 10^{-2}$ rad.), and it reached the web in the next cycle of loading (Photo. 5).

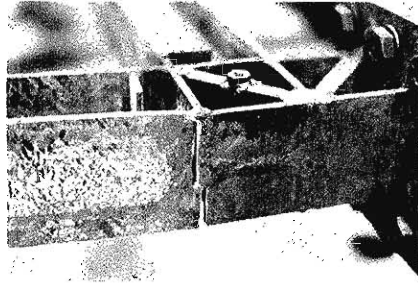


Photo. 5. Crack at the End of Column of BFSO.

4) BFDI

This is the double bracing type specimen whose braces were designed to buckle in the plane of a frame. Experimental $H-\Delta$ relationship is shown in **Fig. 9**. In the first cycle of loading, the braces buckle out of the plane of a frame, i.e., they buckle about the strong axis of a cross section, although the effective slenderness ratio for the buckling about weak axis of cross section is about 44 and that about the strong axis of a cross section is about 36. Maximum load carrying capacity $H=34.7$ t is attained at about $\Delta=0.77$ cm ($R=0.51 \times 10^{-2}$ rad.) in the first cycle of loading. Under subsequent loading of the amplitude $R_d=0.01$, bending deformation about the weak axis of a cross section and the deterioration of load carrying capacity under repeated loading are scarcely observed. In the 5th cycle (1st cycle of $R_d=0.02$), bending deformation about the weak axis of a cross section appears at $R \doteq 0.01$ rad. in the braces subjected to compressive force, as shown by mark ∇ in **Fig. 9**. After that, it becomes predominant, and the deterioration of load carrying capacity due to repeated loading becomes larger. Cracks took place in the flange near the intersecting point of bracing members in the loading of $R_d=0.03$, and it grew in the subsequent loading (**Photo. 6**). The test was terminated when cracks grew severely large.

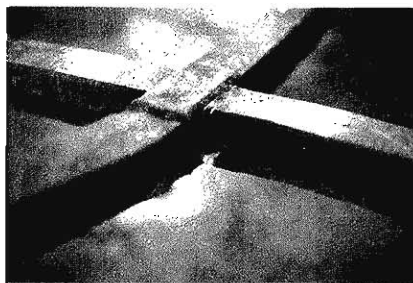


Photo. 6. Cracks at the Center Junction of Braces.

5) BFDO

This is the double bracing type specimen whose braces were designed to buckle in the plane perpendicular to the plane of a frame. The obtained $H-\Delta$ relationship is shown in **Fig. 10**. The maximum load carrying capacity $H=29.23$ t is reached at $\Delta=0.48$ cm ($R=0.32 \times 10^{-2}$ rad.) and the load carrying capacity decreases rapidly after the first buckling of the compressed brace. After the reversal of the direction

of loading the bracing member which was subjected to tensile force in the virgin loading is subjected to compressive force and buckles. The load carrying capacity decreases once slightly after the buckling of this member and it gradually increases until the next unloading point. The hysteresis loops after the second cycle were a hardening type in which slip ranges were contained, as same as in the case of BFDI.

Photo. 7 shows the specimens after tests.

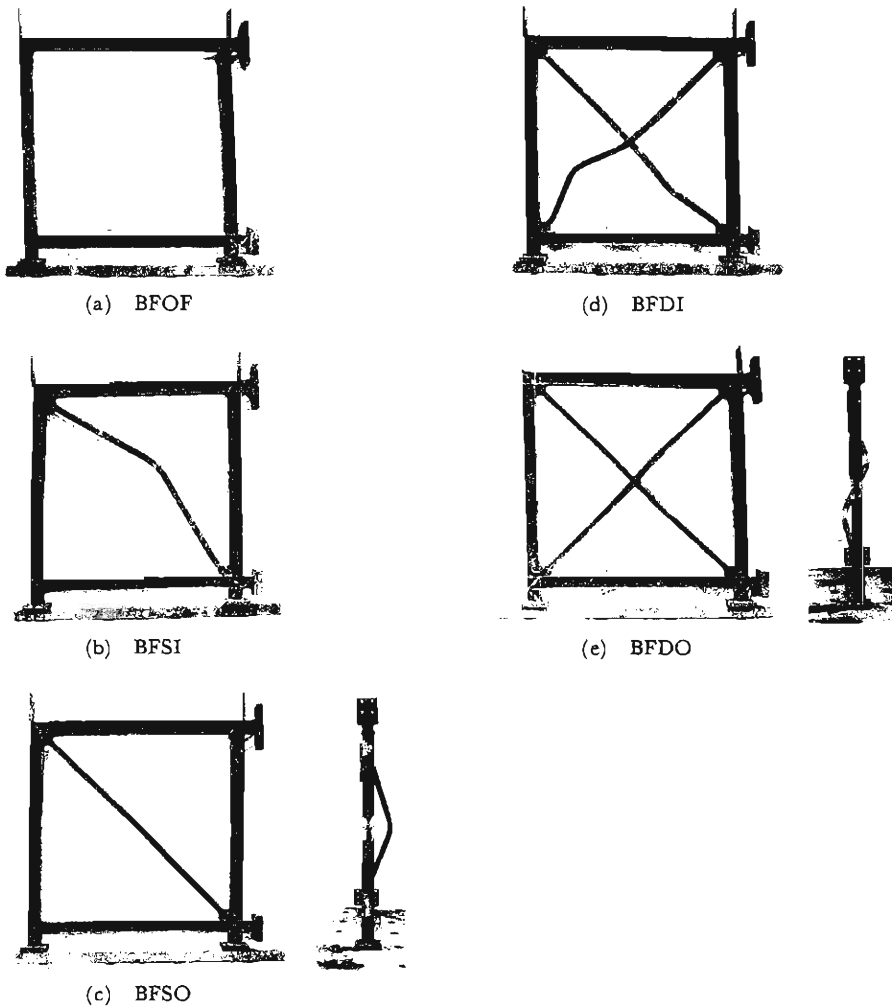


Photo. 7. Test Specimens after Test.

4. Consideration of Test Results

4.1 Hysteretic characteristics of a column

Axial force, bending moment and shear force in columns and beams are calculated from the measured data of strain gages mounted near the mid-length of each

member. Hysteretic characteristics of the axial force and the shear force in the columns are shown in **Figs. 11~15**. Those of the beam ① and the beam ② are quite similar to those of the column ① and the column ②, respectively, although the hysteresis loops are not shown. In the figure, Q_1 and Q_2 represent the shear force in columns ① and ②, and N_1 and N_2 represent the axial force in them, respectively. Axial force is positive when the column is subjected to tensile force, and the positive direction of shear force coincides with that of horizontal force H . The accuracy of the calculated result of the shear force from the data of the strain gages are made

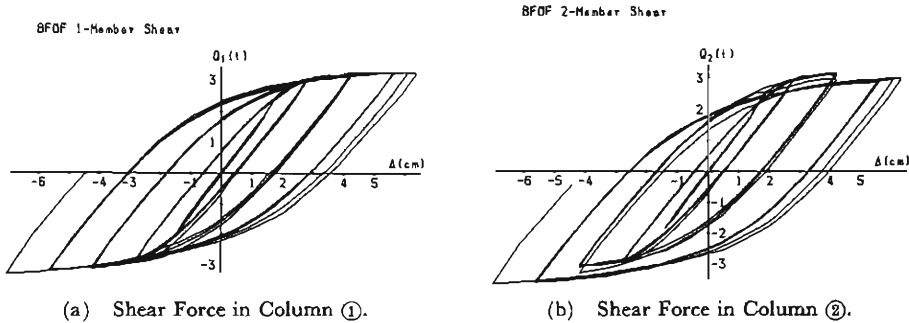


Fig. 11. Stress in the Columns in BFOF.

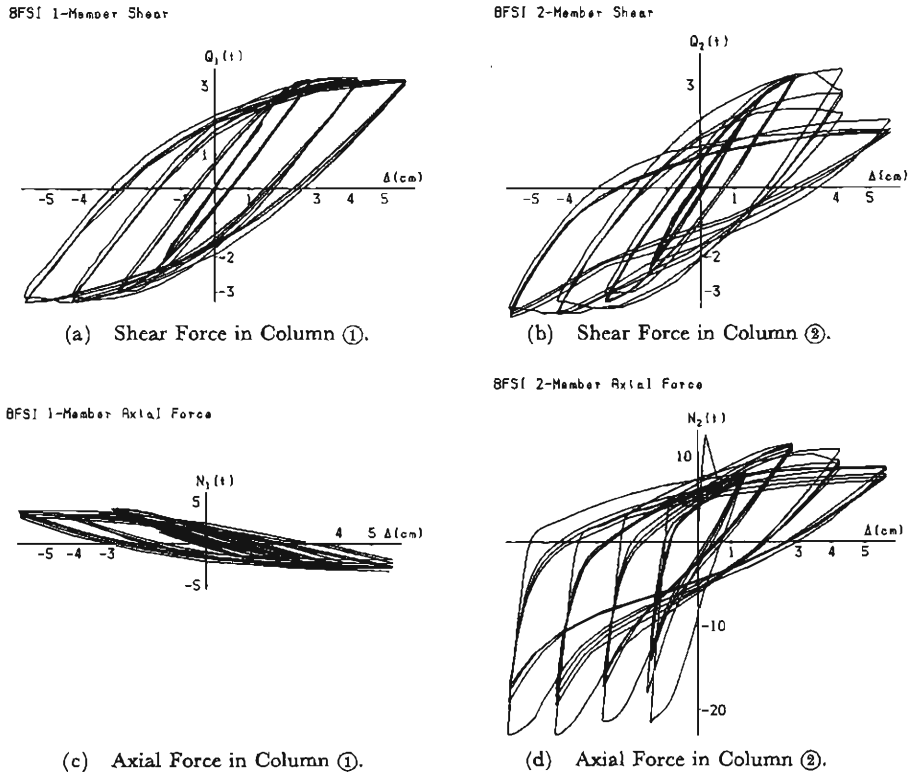


Fig. 12. Stress in the Columns in BFSI.

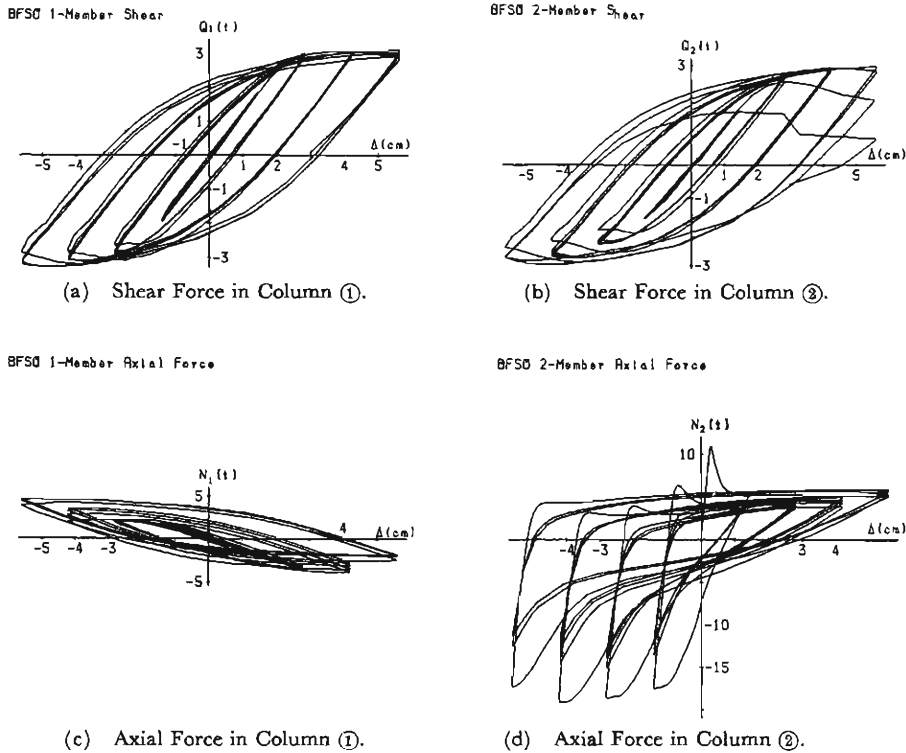
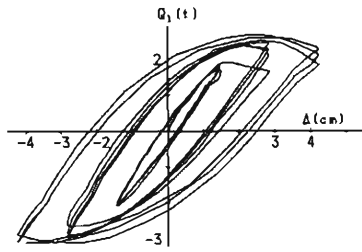


Fig. 13. Stress in the Columns of BFSO.

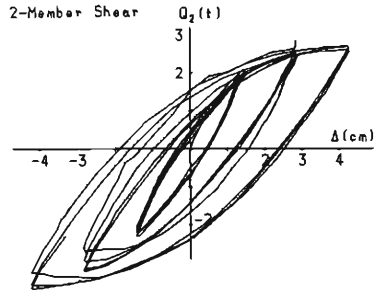
sure from the fact that the sum total of the shear forces in two columns ($Q_c = Q_1 + Q_2$) versus story drift relationship shown by dashed line coincide very well with the horizontal load measured by a load cell versus story drift relationship shown by solid line, as shown in **Fig. 16**. Since the equilibrium condition requires that the axial force in column ① should be equal to the sum of the shear force in beam ② and the vertical component of the axial force in the brace connected at node ①, and that of column ② should be equal to the sum of the shear force in beam ① and the vertical component of the axial force of the brace connected at node ②, the following considerations can be made. In the case of a single bracing system, only column ② is subjected to the effect of axial force of the brace because there is no brace connected at node ①. The hysteresis loop of N_1 - Δ relationship has a spindle shape, resembling that of BFOF. On the other hand, column ② is subjected to large axial force whose greater part is given by a brace. The effect of the variation in the axial force of a brace on the axial force of column ② is observed clearly in **Figs. 12(d)** and **13(d)**. The shape of the hysteresis loop of N_2 - Δ relationship is similar to that of H - Δ relationship. Since, in the case of X-type bracing system, all columns are affected by the axial force of braces, the shape of the hysteresis loop of the N - Δ relationship is similar to that of column ② of the specimen with Z-type bracing. The hysteresis loop of Q - Δ relationship of the column of BFOF and column ① of the specimen with Z-type bracing has a spindle shape, i.e., the load carrying capacity

BFDI 1-Member Shear



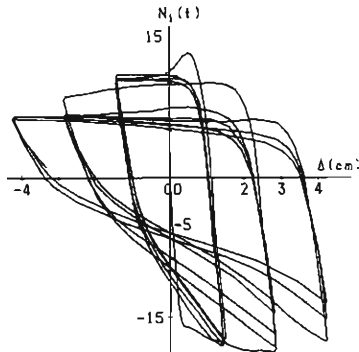
(a) Shear Force in Column ①.

BFDI 2-Member Shear



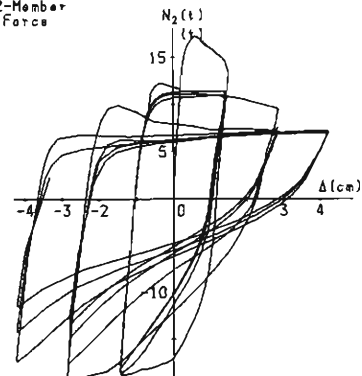
(b) Shear Force in Column ②.

BFDI 1-Member Axial Force



(c) Axial Force in Column ①.

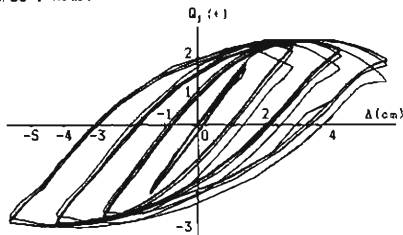
BFDI 2-Member Axial Force



(d) Axial Force in Column ②.

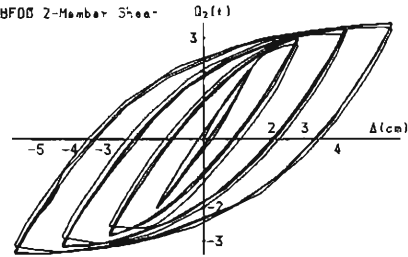
Fig. 14. Stress in the Columns in BFDI.

BFDO 1-Member Shear



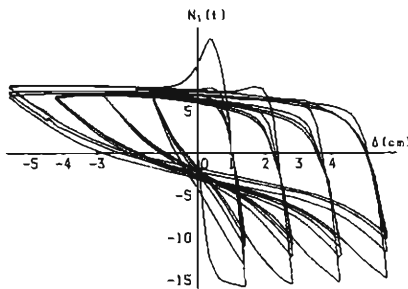
(a) Shear Force in Column ①.

BFDO 2-Member Shear



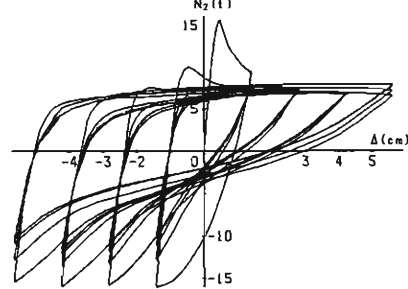
(b) Shear Force in Column ②.

BFDO 1-Member Axial Force



(c) Axial Force in Column ①.

BFDO 2-Member Axial Force



(d) Axial Force in Column ②.

Fig. 15. Stress in the Columns in BFDO.

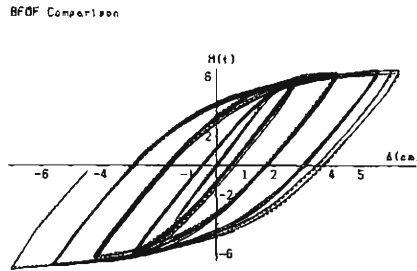


Fig. 16. Comparison between the Load Measured by Load Cell and the Load Calculated from Strain Gage Measurement on Columns.

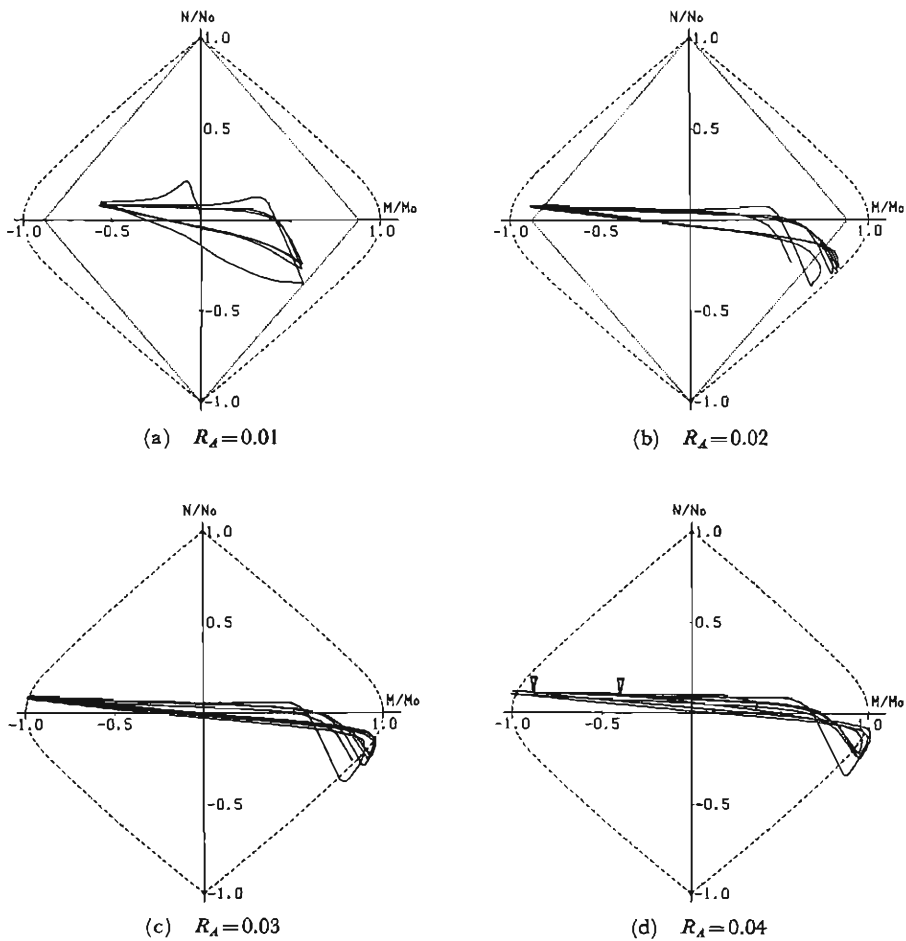


Fig. 17. Stress Paths at the End of Column ② of BFSI.

increases as the story drift increases. However, in the case of braced frames, that of the column in which axial force becomes larger due to the existence of the brace has a different shape from the above mentioned column. The axial compressive force in the column greatly increases especially when the brace becomes straight and yields in tension in the first cycle of each loading amplitude. During the first cycle at each amplitude, first, the shear force increases with the increase of story drift when axial force of the column is relatively small and the column does not yield under the combined stress of axial force and bending moment. As observed in the third quadrant of the (b) figures of **Figs. 12~15**, the shear capacity of the column deteriorates in the range where the brace becomes straight and closes the yielding in tension and the column is subjected to large compressive axial force. Phenomena of this sort can be explained by taking the interaction effect of axial force and bending moment in yielding into consideration. **Figs. 17(a)~(d)** show the axial force in column ② versus bending moment in column ② at the interior top end relationship of BFSO. The dashed line in the figure corresponds to the full plastic state represented by

$$\begin{aligned} \frac{M}{M_0} &= 1 - \left(\frac{N}{N_0} \right)^2 \cdot \frac{A^2}{4t_w Z_p} \\ \text{if } \left| \frac{N}{N_0} \right| &\leq \frac{t_w(D-2t_f)}{A} \\ \frac{M}{M_0} &= \frac{AD}{2Z_p} \left(1 - \left| \frac{N}{N_0} \right| \right) \left\{ 1 - \frac{A}{2BD} \left(1 - \left| \frac{N}{N_0} \right| \right) \right\} \\ \text{if } \left| \frac{N}{N_0} \right| &> \frac{t_w(D-2t_f)}{A} \end{aligned}$$

where N and M are working axial force and bending moment in a column, N_0 is yield axial force, M_0 is full plastic moment in pure bending, Z_p is a plastic modulus and A is a cross sectional area. D and B are the depth of a cross section and the width of flanges, respectively. t_w and t_f are the thickness of web and flange, respectively. The dotted line in the figure represents the condition when a cross section begins to yield under bending and axial force, i.e. $M/M_0 = (Z_e/Z_p)(1 - N/N_0)$, where Z_e is a section modulus. In the loading of $R_d=0.01$, the column is in the elastic state since the generalized stress point ($M/M_0, N/N_0$), lies within the dotted line as shown in **Fig. 17(a)**. In the first cycle of loading of $R_d=0.02$, the trace of generalized stress point crosses the dotted line and the column begins to yield, as shown in **Fig. 17(b)**. It curves as the axial force increases and generalized stress point moves almost parallel to the dashed line, decreasing the moment carrying capacity. Since axial force in the second cycle is not as large as that in the first cycle, the decrease in the moment bearing capacity is scarcely observed and the moment bearing capacity of the column near the unloading point in the second cycle is larger than that in the first cycle of loading. In the loading of $R_d=0.03$ shown in **Fig. 17(c)**, the yield surface seems to expand slightly due to strain hardening effect, however, the decrease in the moment bearing capacity is observed in every cycle of loading. The decrease in the moment bearing capacity is the largest in the first cycle. In the 3rd cycle of $R_d=0.04$, A crack took place at the node ④ and the large amount of decrease in moment bearing capacity is clearly observed in the side of tension loading for the

brace as shown by the marks ∇ in **Fig. 17(d)**. **Fig. 18** shows the comparison of the sum of shear forces in two columns of BFOF (dashed line) with that of BFSI, BFSO, BFDI and BFDO (solid lines). Restoring force of the columns in the braced frame is smaller than that of the pure rigid frame according to the decrease of moment bearing capacity at the ends of the column due to a large axial force from the brace.

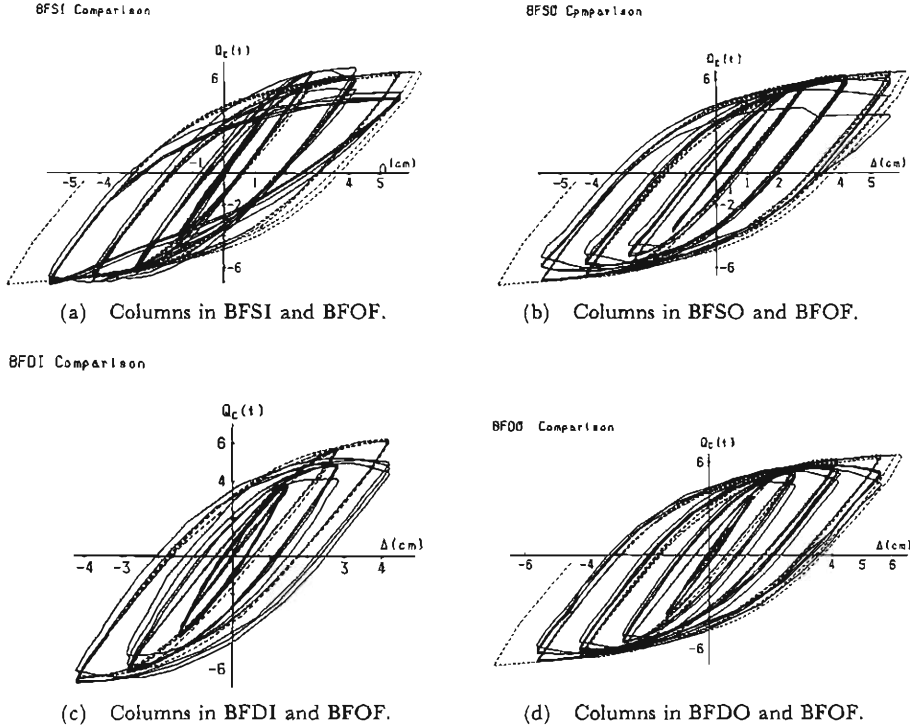


Fig. 18. Comparison of the Behavior of the Column in the Pure Rigid Frame with That of the Braced Frame.

Restoring force of the column was decreased severely due to the initiation of cracks, as shown in **Figs. 12(b)** and **13(b)**. The effect of cracking is first observed as the deterioration of load carrying capacity in the higher side of the curve in the figure. However, it takes place in the lower side in the subsequent loading and the hysteresis loop, which had a spindle shape in the early stage of loading, distorts remarkably.

4.2 Hysteretic Characteristics of the Braces

The horizontal component of the axial force of the brace (Q_b) is easily calculated by the formula $Q_b = H - Q_c$, since the overall load carrying capacity (H) and the load carrying capacity of the columns (Q_c) were already known. The obtained $Q_b-\Delta$ relationships are shown in **Fig. 19** and compared with the test results of the brace members with identical length, which were reported in Part 1¹⁾ in **Fig. 20**. In the figure, the solid line and dashed line represent the result of the present test and the result of Part 1, respectively. The ordinate is non-dimensionalized by the

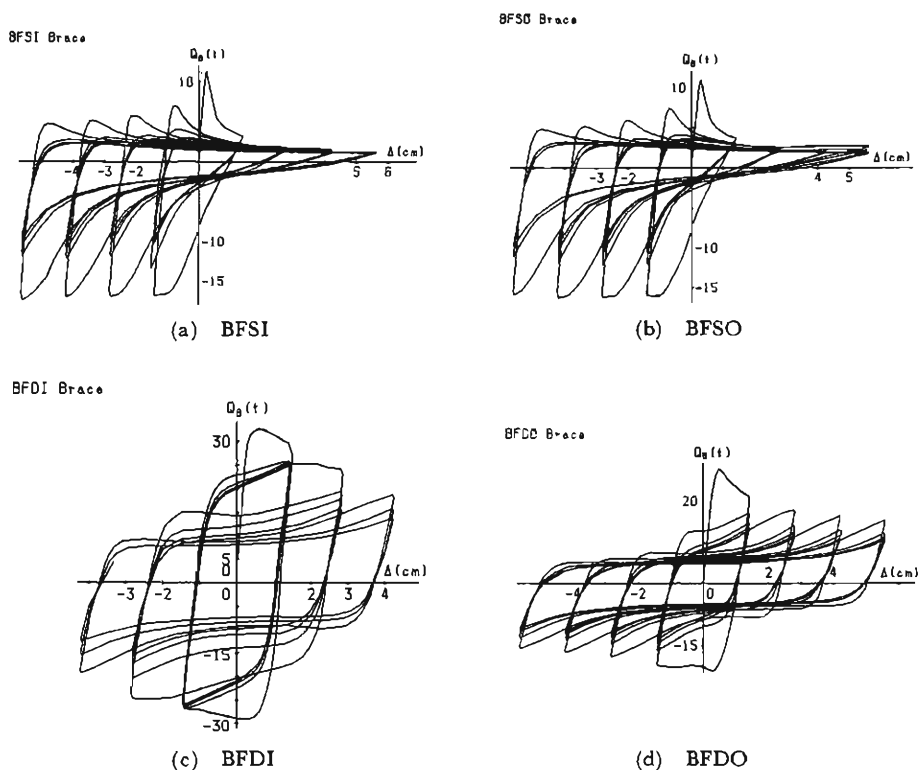


Fig. 19. Restoring Force Characteristics of the Braces in the Braced Frames.

yield horizontal load Q_{By} , which is calculated using the measured dimensions of a cross section and the yield stress which was obtained from the coupon test. In the case of the single bracing system, hysteresis loops of BFSO and SOC 2 match well with one another as shown in **Fig. 20(b)**, although there is a slight difference in the boundary conditions at the ends of the braces. In the case of BFSI and SIC 2, the match is also good in the range of $R_A \leq 0.02$. However, the tensile load carrying capacity of SIC 2 becomes lower than that of BFSI in the loading of $R_A = 0.03$ because of the initiation of cracks near the end of the brace of SIC 2. Direct comparison of BFDI with DIC 2 can not be made because BFDI buckled and deformed about the strong axis of a cross section in the loading of $R_A = 0.01$, although it was designed to buckle about the weak axis of a cross section. After the second cycle of $R_A = 0.02$ loading, bending deformation about the weak axis was dominant and the behaviors of BFDI and DIC 2 began to resemble each other. Cracks took place in both specimens in the loading of $R_A = 0.03$. The crack initiation of DIC 2 was earlier than that of BFDI and the load carrying capacity of DIC 2 decreased more largely than that of BFDI. In the case of BFDO and DOC 2, the type of hysteresis loops of both specimens are hardening types in which slip ranges are contained. The buckling load of BFDO is smaller than that of DOC 2, because the effective slenderness ratio of the braces in BFDO is slightly larger than that of DOC 2 due to the difference in boundary conditions, as explained later.

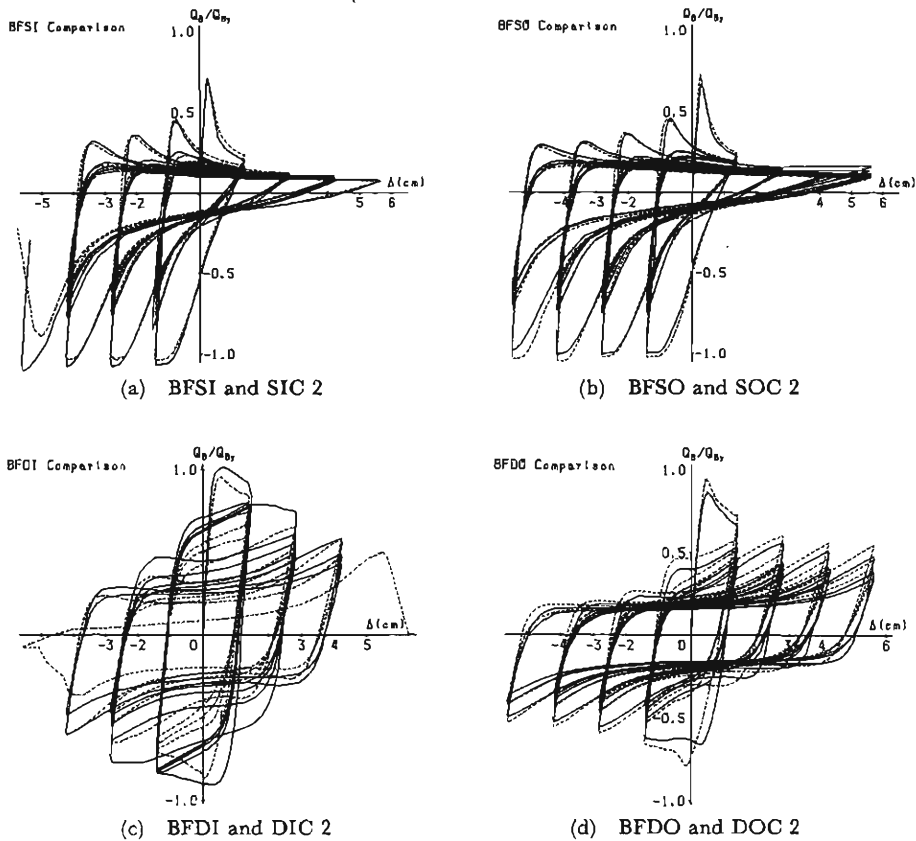


Fig. 20. Comparison of the Behavior of the Braces in the Present Test with That of the Braces Reported in Part 1.

Although the effective lengths of the braces for buckling are different between the present test and the test reported in Part 1¹⁾ in the exact sense because the rigidities of the surrounding frames are different, it is recognized in **Figs. 20(a)~(b)** that the post-buckling and hysteretic behaviors of the braces are not affected largely as a whole.

4.3 Effective Slenderness Ratio of the Braces

Effective slenderness ratio of the braces reported in Part 1¹⁾ was calculated by solving an eigen value problem using the slope deflection method in which the secondary effect of axial force was taken into consideration. Supporting condition of the brace was assumed to be fixed completely in the formulation of the basic equations because a cross section of the beams and the columns of the surrounding frame were much larger than that of the brace. In the case of this experiment, however, as the cross section of the beams and the columns, respectively are not much larger than that of the brace, the effect of the deformation of the surrounding frame might be needed to be taken into account to calculate the effective slenderness ratio of the brace.

In the case of BFSI, the nodes ② and ④ of the surrounding frame are subjected to moments with equal magnitude (M) and opposite sign due to the deformation of a brace. The relationship between the moment (M) and the relative rotation angle of the nodes (θ) is represented by the equation $M = (8E_c I_c / l_c) \cdot \theta$, where E_c , I_c and l_c are the Young's modulus, moment of inertia of a cross section of the column and the length of the column, respectively. Elastic buckling load or effective slenderness ratio of a brace can be calculated using the rotational rigidity (M/θ). The calculated effective slenderness ratio (λ_e) is 80.9 for the case of BFSI. On the other hand, the slenderness ratio of the fixed ended brace with the same length is 80.4, using the nominal dimensions in calculation. λ_e is 0.6% larger than λ . The difference between λ_e and λ is very small. The effective slenderness ratio was analysed to examine the effect of the rotational restraint at the ends of the braces by the surrounding frame. The results of the analysis are shown in Fig. 21. The ordinate denotes the calculated ratio of the effective slenderness ratio to the slenderness ratio which is calculated under the assumption that the brace is rigidly fixed at the ends. The abscissa denotes the ratio (k) of the flexural rigidity (I/l) of the beam and the column against in-plane loading to that of the brace. In the case of X-type bracing system, the effective slenderness ratio of the compressed brace could be calculated by taking not only the rigidity of the surrounding frame but also the rigidity of the intersected tension brace against the in-plane rotation into consideration, as shown in Fig. 21(b).

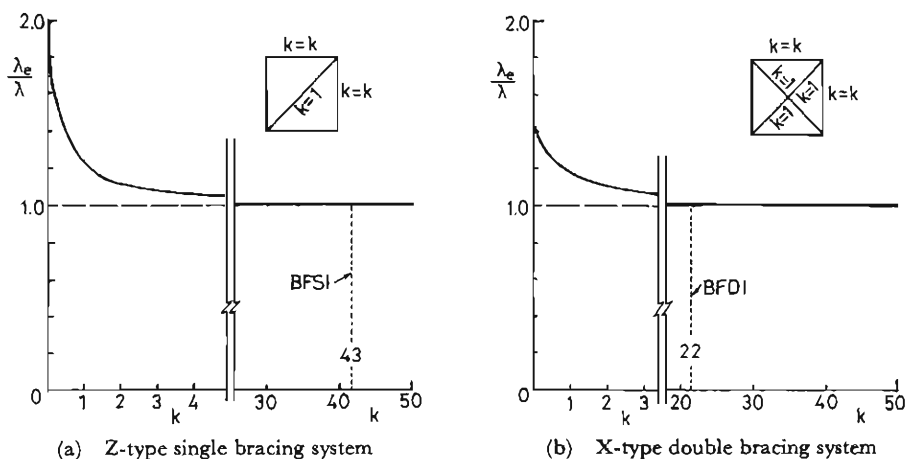


Fig. 21. Results of Analysis of the Effect of the End Restraint by the Surrounding Frame.

4.4 Effect of Local Behavior

As reported in Part 1¹⁾ and Part 2²⁾, local buckling takes place in the case of those braces with a thin walled section in the comparatively early stage of loading and it induces cracks and breakage of the member under cyclic loading. In the present test, cracks took place at the intersection of bracing members in the case of BFDI. In the case of BFSI, cracks took place not only at the end of a column but also at the end of braces where the discontinuity of the cross sectional shape is severe, as shown in Photo. 4. In the cases of the braces of BFDI and BFDO, which were

designed to buckle out of the plane of a frame, cracks in the braces were not observed during the tests. Referring to the result in Part I¹⁾, cracks might take place more easily in the case of the braces designed to buckle in the plane of a frame than those designed to buckle out of the plane of a frame. In the cases of BFSI and BFSO, cracks in the columns took place near the welded portion, i.e., at the thermally affected portion due to welding. As described in the previous section 4.2, the initiation of a crack decreases the load carrying capacity of the system.

5. Concluding Remarks

On the behavior of the braced frames tested here, the following remarks can be drawn.

(1) The effective slenderness ratio of the braces which buckles within the plane of a frame could be estimated by the use of the slope deflection method taking into account the secondary effect of axial force and the rotational constraints at the ends by the surrounding frame. In the case of the rigid frame whose columns and beams have comparatively large cross sectional dimensions comparing with those of a brace, an assumption that braces would be rigidly fixed against end rotation by the members of a surrounding frame would not induce a large inaccuracy in the estimation of the effective slenderness ratio, unless the slenderness ratio of the brace is very small.

(2) Since it is recognized from the result of comparison of the behavior of the brace with that reported in Part I¹⁾ that there are not large qualitative and quantitative differences between the post-buckling and hysteretic behaviors of the braces reported in Part I¹⁾ and those of the present tests, braces could be treated as a bar which is rigidly fixed at the ends and subjected to only an axial force except in the estimation of buckling strength, neglecting the effect of the rotational rigidity at the ends due to the surrounding frame.

(3) If a column is not subjected to the axial load due to the existence of braces, the axial force in the column is relatively small and the hysteresis loop of the restoring force versus story drift relationship is a spindle shape and is very stable under repeated loading. However, in the case of the column which is subjected to the axial force from the brace, the moment bearing capacity at the critical sections in the column decrease, according to the interaction characteristics in yielding under combined bending and axial thrust, as the axial force in the column becomes larger. Under the prescribed constant amplitude loading, the axial force in the column is largest in the first cycle of loading of each prescribed amplitude, since the brace is stretched and yields in tension in the first cycle but is not stretched completely and does not yield in and after the second cycle. Hence, decrease in load carrying capacity of columns is largest in the first cycle of each amplitude, and the load carrying capacity becomes larger and the hysteresis loop becomes to resemble a spindle shape in and after the second cycle of loading.

(4) The ductility of the structure was exhausted when cracks took place in a brace or a column. The crack in a brace takes place due to low cycle fatigue phenomenon at the locally buckled portion or at the portion near the tip of gusset plate where discontinuity of a cross section exists and notch effect due to stress concentration is large. The crack in a column takes place near the welded portion, i.e., at the portion affected thermally by welding.

After the crack initiation in the flange of a column, the load carrying capacity of the column decreases largely only in one direction of loading under which the cracked flange is subjected to tensile force. When cracks reach the web, the load carrying capacity in another direction begins to decrease and the shape of hysteresis loop becomes quite different from a spindle shape, having a kink. In the subsequent loading, the column would encounter breakage and failure.

References

- 1) Wakabayashi, M., T. Nakamura and N. Yoshida; Experimental Studies on the Elastic-Plastic Behavior of Braced Frames under Repeated Horizontal Loading, Part 1, Experiments of Braces with an H-shaped Cross Section in a Frame, Bull. Disas. Prev. Inst., Kyoto University, Vol. 27, Part 3, No. 251, September 1977, pp. 121-154.
- 2) Wakabayashi, M., T. Nakamura and N. Yoshida; Experimental Studies on the Elastic-Plastic Behavior of Braced Frames under Repeated Horizontal Loading, Part 2, Experiments of Braces Composed of Steel Circular Tubes, Angle-Shapes, Flat Bars or Round Bars, Bull. Disas. Prev. Inst., Kyoto University, Vol. 29, Part 3, No. 264, March 1980, pp. 99-127.